Journal of Biomechanics 49 (2016) 401–407

Contents lists available at ScienceDirect

Journal of Biomechanics

journal homepage: www.elsevier.com/locate/jbiomech
www.JBiomech.com

Oriented cell division affects the global stress and cell packing geometry of a monolayer under stretch

Guang-Kui Xu [a,*], Yang Liu [a], Zhaoliang Zheng [b]

[a] International Center for Applied Mechanics, State Key Laboratory for Strength and Vibration of Mechanical Structures, School of Aerospace, Xi'an Jiaotong University, Xi'an 710049, China
[b] Stephenson Institute for Renewable Energy, Department of Chemistry, University of Liverpool, Crown Street, Liverpool L69 7ZD, UK

ARTICLE INFO

Article history:
Accepted 30 December 2015

Keywords:
Cell division
Vertex dynamics models
Cell geometry
Monolayer

ABSTRACT

Cell division plays a vital role in tissue morphogenesis and homeostasis, and the division plane is crucial for cell fate. For isolated cells, extensive studies show that the orientation of divisions is sensitive to cell shape and the direction of extrinsic mechanical forces. However, it is poorly understood that how the cell divides within a cell monolayer and how the local stress change, due to the division, affects the global stress of epithelial monolayers. Here, we use the vertex dynamics models to investigate the effects of division orientation on the configurations and mechanics of a cell monolayer under stretch. We examine three scenarios of the divisions: dividing along the stretch axis, dividing along the geometric long axis of cells, and dividing at a random angle. It is found that the division along the long cell axis can induce the minimal energy difference, and the global stress of the monolayer after stretch releases more rapidly in this case. Moreover, the long-axis division can result in more random cell orientations and more isotropic cell shapes within the monolayer, comparing with other two cases. This study helps understand the division orientation of cells within a monolayer under mechanical stimuli, and may shed light on linking individual cell's behaviors to the global mechanics and patterns of tissues.

1. Introduction

The formation and development of animal tissues requires the coordinated movements of their constituent cells, including cell growth, cell intercalation, and cell division (Lecuit and Lenne, 2007; Heisenberg and Bellaïche, 2013; Guillot and Lecuit, 2013). Among these cellular processes, cell division can dictate the topological disorder in epithelia (Gibson et al., 2006), control the homeostatic cell packing geometry (Ragkousi and Gibson, 2014), and drive the morphogenesis of tissues (Kondo and Hayashi, 2013). Furthermore, the cell division axis determines the future positions of daughter cells, and is crucial for the cell fate (Théry et al., 2005).

In recognition of its significance in biological functions, much effort has been directed toward investigating the orientation of cell division under different microenvironments (Théry et al., 2005; Fink et al., 2011; Gibson et al., 2011; LeGoff et al., 2013). At the cellular level, cell shape is thought to dictate the orientation of the division plane that mitotic cells tend to divide orthogonal to their geometric long axis (Hofmeister, 1863; Gray et al., 2004; Strauss et al., 2006). Recently, Fink et al. (2011) experimentally showed that the external force can bias dynamic subcortical actin structures, resulting in the alignment of daughter cells with the external force field. Moreover, the effect of geometric constraints from microenvironments (e.g., extracellular matrix) on the cell division orientation has been examined (Théry et al., 2005; Minc et al., 2011). In these studies, attentions have been mainly paid to the unicellular systems. To date, however, little is known about the orientation of cell division within a cell monolayer, where the cell geometry does not exist in isolation. Harris et al. (2012, 2013) developed a testing device to characterize the mechanical properties of freely suspended epithelial monolayers. Interestingly, using this device, Wyatt et al. (2015) found that when the epithelia was subjected to a stretch, the cell divided aligning with its geometric long axis, rather than with the stretching axis. In spite of these studies, the mechanisms governing the orientation of cell division in different microenvironments remain unclear, and understanding how the local changes at cellular level affects the tissue-scale mechanical properties is still a challenge.

Various theoretical and computational techniques, such as Cellular Potts models (Graner and Glazier, 1992; Käfer et al., 2007), Flocking models (Basan et al., 2013; Sepúlveda et al., 2013) and phase field methods (Camley et al., 2014), have been developed to study the spatial and temporal evolution of cells within epithelial monolayers. Among them, vertex dynamics models have proven to be a powerful

* Corresponding author.
E-mail address: guangkuixu@mail.xjtu.edu.cn (G.-K. Xu).

http://dx.doi.org/10.1016/j.jbiomech.2015.12.046
0021-9290/

tool to study the epithelial morphogenesis and cellular biological processes within epithelia (Farhadifar et al., 2007; Rauzi et al., 2008; Marinari et al., 2012; Fletcher et al., 2014; Xu et al., 2015). By using this approach, Marinari et al. (2012) showed that the cell delamination could relieve the overcrowding-induced anisotropy of a tissue. Rauzi et al. (2008) used this method to study the role of the tension anisotropy in driving tissue elongation, and compared their predictions with experimental observations. This approach also verified the experimental results that the apoptotic cells could drive the folding of epithelia (Monier et al., 2015) and the rosette formation during the apical-contraction phase (Kuipers et al., 2014).

In this paper, we employ the vertex dynamics models to investigate the orientation of cell division within an epithelial monolayer under stretch, and show how the local topology change of dividing cells influences the global stress and cell packing of the monolayer. It is found that the cell division aligns with the long axis of cell shapes, rather than with the stretching direction or at a random orientation. Furthermore, the global stress of cell monolayers releases more rapidly when the cell divides along its long axis. Finally, the geometric long-axis division can result in a more random cell packing orientations and more isotropic cell shapes, comparing with other two division options.

2. Models

2.1. Model of the cell monolayer

Consider a large number of cells forming a confluent monolayer sheet, in which the cell shape is affected by its adjacent cells. In vertex dynamics models, each cell in the monolayer is modeled as a polygon with vertices and edges shared between adjacent cells (see Fig. 1(a)). The locations of the vertices and edges provide complete information about the configuration of cell sheet. Based on this framework, the vertex dynamics models describe the movement of cell position and the change in cell shape by using the motion of vertices. Suppose the monolayer consists of N' cells, numbered by $\alpha = 1, 2, ..., N'$, and the cell packing geometry is denoted by N vertices, numbered by i=1, 2, …, N. As described by Farhadifar et al. (2007), the total free energy U of the cell monolayer is summarized as

$$U = \sum_{\alpha} \frac{K_e}{2}(A_\alpha - A_0)^2 + \sum_{\langle ij \rangle} K_l l_{ij} + \sum_{\alpha} \frac{K_c}{2} L_\alpha^2 \quad (1)$$

where K_e is the elastic modulus of the cell, A_α and L_α are the area and perimeter of the $\alpha-$ thcell, A_0 is the preferred cell area, l_{ij} denotes the length of the edge connected by vertices i and j, $\sum_{\langle ij \rangle}$ summates all adjacent vertices, K_l represents the strength of line tension between cells, and K_c represents the cortical elasticity of cellular perimeters. In Eq. (1), the first term describes the elastic energy of the cell, with K_e being the elastic stiffness. The second term denotes the interactions between adjacent cells, including the adhesion energy released by the binding of E-cadherin molecules and the deformation energy of subcortical actin cytoskeleton (Farhadifar et al., 2007). The binding of adhesion molecules releases energy, which prefers a longer cellular edge, whereas the deformation of actin cytoskeleton increases the energy, favoring a shorter cellular edge. Therefore, the value of K_l could be positive or negative, which depends on the competition between the adhesion interaction of cells and the deformation energy of actin cytoskeleton. The last term represents the contribution of the active contractility of actin-myosin rings. The epithelial cell forms an actin-myosin belt that tends to span the entire cell (Farhadifar et al., 2007). The force F_i acting on the $i-$ th vertex is determined by the negative gradient of the energy with respect to the coordinates r_i of this vertex

$$F_i = -\frac{\partial U}{\partial r_i} \quad (2)$$

Suppose the polygonal vertex positions r_j (j=1, …, n) of the $\alpha-$ th cell are ordered in counter-clockwise direction, where n is the number of vertices of this cell. The cellular area can be calculated by $A_\alpha = (1/2)\sum_{j=1}^{n} |r_j \tilde{n} r_{j-1}|$, considering $r_0 = r_n$. The length of each cellular edge is $l_j = |r_j - r_{j-1}|$, and the cellular perimeter is $L_\alpha = \sum_{j=1}^{n} l_j$. Each vertex i is surrounded by three neighboring vertices (k=1, 2, 3) and by three neighboring cells (β=1′, 2′, 3′), as illustrated in Fig. 1(b). With these geometric information, we can obtain the forces acting on vertex i in x and y directions

$$F_{i,x} = -\frac{K_e}{2}[(A_{1'} - A_0)(y_2 - y_3) + (A_{2'} - A_0)(y_3 - y_1) + (A_{3'} - A_0)(y_1 - y_2)]$$

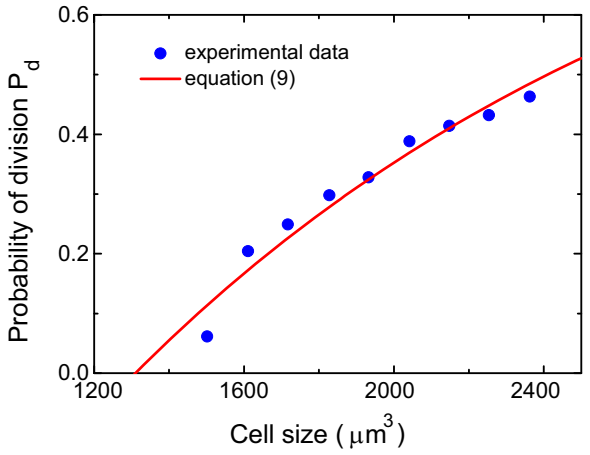

Fig. 2. Probability of cell division as a function of the cell size. The probability division function (solid line) fits with the experimental data (dots) from Tzur et al. (2009). By taking the preferred volume $V_0 = 1000$ μm^3, the fitted parameters are $\kappa = 0.63$ and $V_d = 1.3\ V_0$.

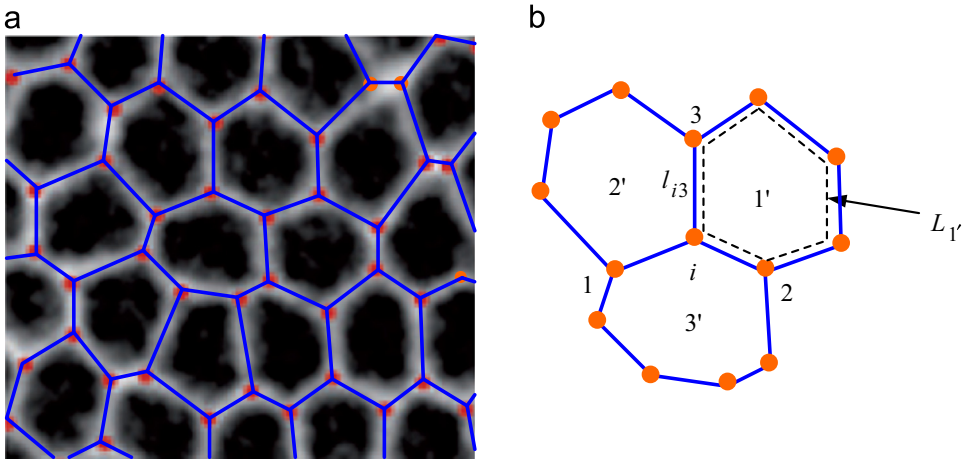

Fig. 1. Illustration of vertex dynamics models. (a) Cell shape within a epithelial monolayer sheet, adapted from the literature (Lecuit and Lenne, 2007). (b) Description of cell shapes. Each cell in the monolayer is modeled as a polygon with vertices and edges shared between adjacent cells. Each vertex (i) has three neighboring vertices and three neighboring cells.

$$-K_l\sum_{k=1}^{3}\frac{(x_i-x_k)}{l_{ik}}-2K_c\left[\frac{x_i-x_1}{l_{i1}}(L_{2'}+L_{3'})\right.$$
$$\left.+\frac{x_i-x_2}{l_{i2}}(L_{1'}+L_{3'})+\frac{x_i-x_3}{l_{i3}}(L_{1'}+L_{2'})\right] \quad (3)$$

$$F_{i,y}=-\frac{K_e}{2}\left[(A_{1'}-A_0)(x_2-x_3)+(A_{2'}-A_0)(x_3-x_1)+(A_{3'}-A_0)(x_1-x_2)\right]$$
$$-K_l\sum_{k=1}^{3}\frac{(y_i-y_k)}{l_{ik}}-2K_c\left[\frac{y_i-y_1}{l_{i1}}(L_{2'}+L_{3'})\right.$$
$$\left.+\frac{y_i-y_2}{l_{i2}}(L_{1'}+L_{3'})+\frac{y_i-y_3}{l_{i3}}(L_{1'}+L_{2'})\right] \quad (4)$$

Because the inertia of cells can be neglected, the evolution of the position r_i of each vertex i in the viscous monolayer is given by

$$\eta\frac{\mathrm{d}r_i}{\mathrm{d}t}=F_i(t) \quad (5)$$

where η is the frictional coefficient, and $F_i(t)$ is the total force acting on the vertex i at time t. In addition, the experimental fluctuation is introduced to avoid the system trapped in a local minimum. The random forces F_R are added in the simulations through (Li and Sun, 2014)

$$\langle F_{R,a}(t)F_{R,b}(t')\rangle=\gamma^2\delta(t-t')\delta_{ab} \quad (6)$$

where γ characterizes the magnitude of the fluctuation, $\delta(t)$ and δ_{ab} are Dirac's and Kronecker's $\delta-$functions. For a cell with index α, its stress tensor can be calculated by (Ishihara and Sugimura, 2012; Sugimura and Ishihara, 2013)

$$\sigma^{\alpha}_{mn}=\frac{K_e(A_\alpha-A_0)A_\alpha+\sum_{[\alpha\beta]}\left[K_l+K_c\left(L_\alpha+L_\beta\right)\right]l^m_{\alpha\beta}l^n_{\alpha\beta}/|l_{\alpha\beta}|}{A_\alpha} \quad (7)$$

where (m, n) are the indices for (x, y), $\sum_{[\alpha\beta]}$ runs over all adjacent cells with index β of the $\alpha-$th cell, and $l_{\alpha\beta}=\left(l^x_{\alpha\beta},\ l^y_{\alpha\beta}\right)$ is the vector of the edge shared by the $\alpha-$th and $\beta-$th cells. Then, the stress tensor of the global cell monolayer is written as

$$\sigma_{mn}=\frac{\sum_\alpha K_e(A_\alpha-A_0)A_\alpha+\sum_\alpha\sum_{[\alpha\beta]}\left[K_l+K_c\left(L_\alpha+L_\beta\right)\right]l^m_{\alpha\beta}l^n_{\alpha\beta}/2|l_{\alpha\beta}|}{\sum_\alpha A_\alpha} \quad (8)$$

2.2. Modeling cell division

As observed in experiments (Chen et al., 1997; Tzur et al., 2009), the cell division depends on its geometric size, and the division probability increases with the cell size. To account for this phenomenon, we simulate the likelihood of cell division by using the function

$$P_d=1-\exp\left(\kappa\frac{A_d-A_\alpha}{A_0}\right) \quad (9)$$

where A_α is the cell area, and A_d is a parameter controlling the onset of the cell division, below which the division does not occur, and κ is a parameter controlling the division probability.

In analogy, we can assume the probability function of cell division in three dimensions: $P_d=1-\exp\left[\kappa(V_d-V_\alpha)/V_0\right]$, where V_α, V_d, and V_0 are corresponding volume parameters, respectively. To verify the validity of this division function, we fit this equation to the experimental data from Tzur et al. (2009), who measured the division likelihood as a function of cell volume. By taking the preferred volume $V_0=1000\ \mu m^3$, this division function fits well the experimental data for all measured cell sizes, as shown in Fig. 2. From the fitting, we can obtain the parameters $\kappa=0.63$ and $V_d=1.3\ V_0$. Since the height of each cell is almost the same in the monolayer, the parameters $\kappa=0.63$ and $A_d=1.3\ A_0$ in Eq. (9) will be used throughout this paper for a two dimensional cell sheet. Although not be quantitative, Eq. (9) can capture the essential relation between the division probability and the cell size. In our simulations, if the cell area is larger than A_d, we calculate the probability P_d. The cell division occurs if a generated random number is smaller than the value of P_d.

3. Results and discussions

We normalize the system by the length scale $\sqrt{A_0}$, the time scale $\eta/\left(K_e\sqrt{A_0}\right)$, and the force scale $K_eA_0^{3/2}$. Farhadifar et al.

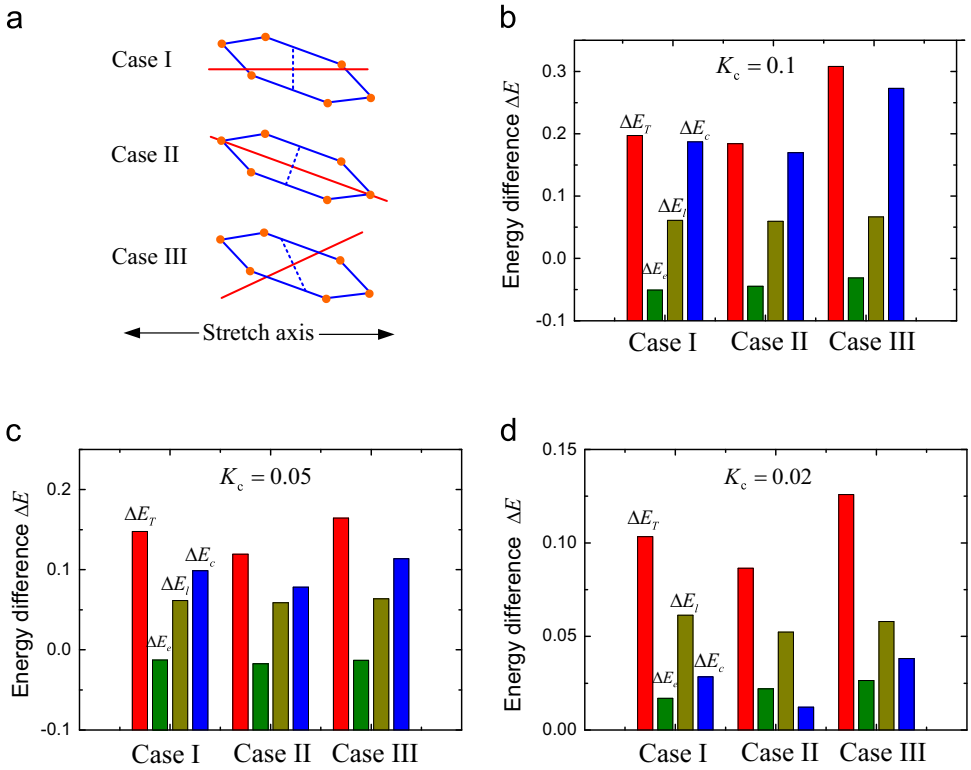

Fig. 3. (a) Three cases of cell division: (I) dividing along the stretch axis, (II) dividing along the long cell axis, and (III) dividing at a random orientation. Different energy terms in three division cases for different contractive ability: (b) $K_c=0.1$, (c) $K_c=0.05$ and (d) $K_c=0.02$. The terms ΔE_T, ΔE_e, ΔE_l, and ΔE_c represent the average of total energy difference, area elastic energy difference, line energy difference, and contractive energy difference between a mother cell and its two daughter cells, respectively. (For interpretation of the references to color in this figure, the reader is referred to the web version of this article.)

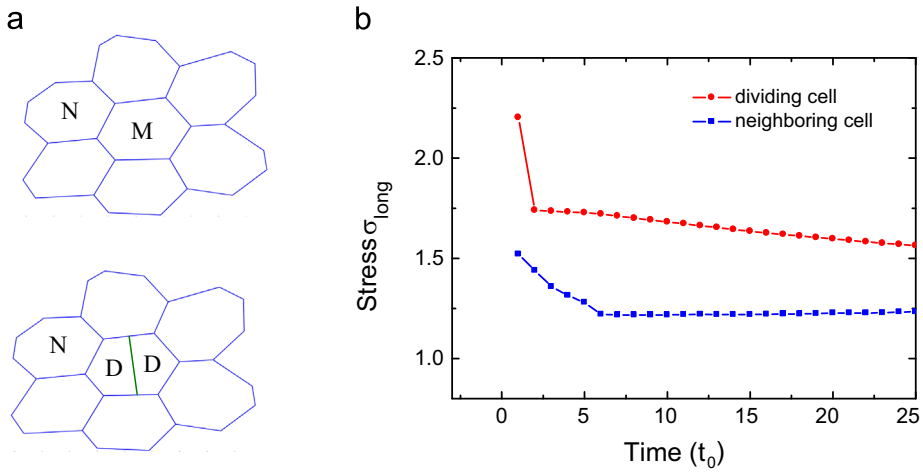

Fig. 4. (a) Snapshots of a dividing cell and its adjacent cells. The mother cell, daughter cell and neighboring cell are denoted by the symbols M, D, and N, respectively. (b) The stresses of a daughter cell (red) and a neighboring cell (blue) along their long axis are plotted as a function of time t for a short time interval. t_0 is a unit of simulation time. (For interpretation of the references to color in this figure legend, the reader is referred to the web version of this article.)

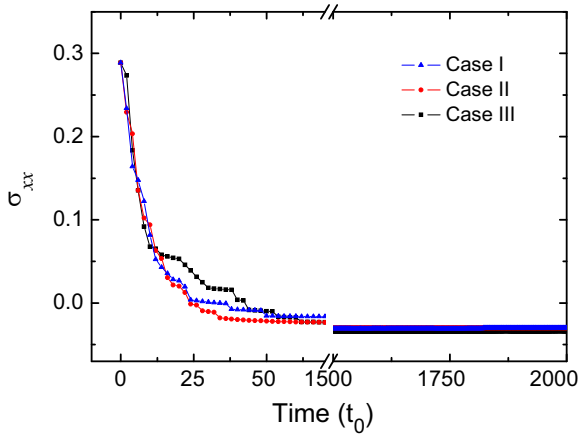

Fig. 5. Global stress σ_{xx} of the cell monolayer in the stretching direction with respect to the time t. The blue, red and black lines represent that the cell divides in Cases I, II, and III, respectively. t_0 is a unit of simulation time. (For interpretation of the references to color in this figure legend, the reader is referred to the web version of this article.)

(2007) used the vertex dynamics model to study the physical basis of epithelial cell packing geometry and compared the predictions with their experimental observations. They showed the parameter region to obtain the stable cell network systems that can support the stretch. Our previous work (Xu et al., 2015) also showed the parameters to capture the essential mechanical properties of cells. Based on these work, we take the preferred area of cells $A_0 = 1$, the line tension $K_l = 0.05$, and the magnitude of the fluctuation $\gamma = 0.02$ in this study. Unless otherwise noted, the parameter of cortical elasticity is set to be $K_c = 0.1$. Firstly, we put 100 cells in a box with size 10×10, and describe the cell geometric shapes by using Voronoi tessellations (Li and Sun, 2014; Wilk et al., 2014). The periodic boundary conditions are applied in both x and y directions. Then, the box size has been relaxed until the system arrives at equilibrium, where the relative difference between the free energies of the system at two neighboring steps is smaller than 10^{-7}. At equilibrium, we have 136 cells and the box size is 10.4×11.4. In the present study, we stretch uniaxially the system, and the movement of vertices and the division of cells will lead to a new geometric configuration of the system.

3.1. Division orientation of cells within a monolayer under stretch

Wyatt et al. (2015) experimentally showed that the cell within a monolayer divides along the long cell axis to dissipate the tensile stress, while Fink et al. (2011) demonstrated that the tension can orient the cell division along the tensile direction. To study the division orientation of cells within a monolayer under stretch, we here consider three scenarios of the divisions: (I) the cell divides along the stretch direction, (II) the cell divides along its geometric long axis, and (III) the cell divides at a random orientation, as illustrated in Fig. 3(a). The monolayer is uniaxially stretched by a 30% strain, as done in the experiments (Wyatt et al., 2015).

To examine the effects of different energy terms, we calculate the averages of the total energy difference ΔE_T, area elastic energy difference ΔE_e, line energy difference ΔE_l and contractive energy difference ΔE_c between a mother cell and its two daughter cells over all divided cells. Fig. 3(b) shows the different energy differences in three cases of division orientation. The red, olive, dark yellow, and blue columns represent the energy differences ΔE_T, ΔE_e, ΔE_l, and ΔE_c, respectively. It can be seen that in three cases, the randomly divided orientation (Case III) creates the maximal increase in total energy ΔE_T (Red). The total energy difference is basically the same in Cases I and II but a bit smaller in Case II. This result means that the oriented cell division along the long axis takes the minimal increase in total energy. As shown in Fig. 3(b), the contractive energy difference (Blue) plays a dominant role in determining the total energy difference . The newly generated edge between two daughter cells is smallest in Case II, and thus, the energy difference is minimal. Therefore, the cell in the monolayer prefers to dividing along its long axis, as observed in experiments (Wyatt et al., 2015).

We use different values of K_c to further examine the effect of the contractive ability of actin-myosin rings. A larger value of K_c means a stronger contraction of actin-myosin rings. By taking $K_c = 0.1$, $K_c = 0.05$, and $K_c = 0.02$, the corresponding energy differences during the division are plotted in Fig. 3(b)–(d), respectively. It is found that for three different values of K_c, is always smallest in Case II, meaning cells tend to divide along its long axis. In addition, as the molecular contractive strength decreases (e.g., $K_c = 0.02$), the contribution of ΔE_c to ΔE_T becomes smaller, and the difference of the values of in three cases is also smaller (see Fig. 3 (d)), comparing with the three cases in Fig. 3(b). This result

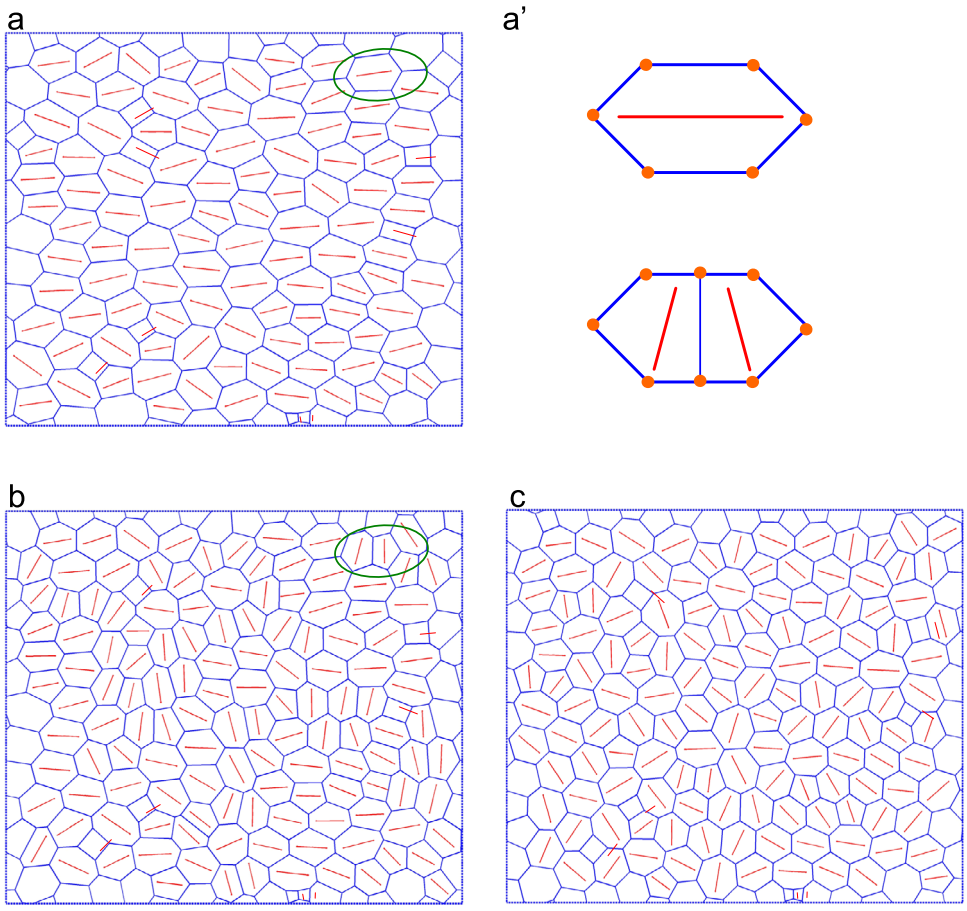

Fig. 6. Cellular configuration within the monolayer with respect to the time: (a) $t=0$, (b) $t=10\ t_0$, and (c) $t=2000\ t_0$. The cartoon in (a') illustrates the orientation change when a mother cell divides into two daughter cells.

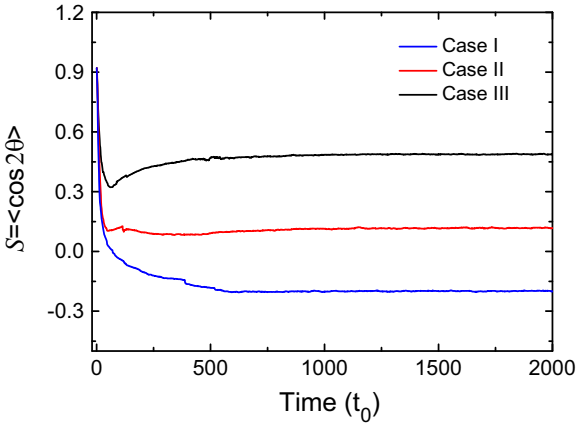

Fig. 7. Order parameter $S=\langle\cos 2\theta\rangle$ as a function of the simulation time t. The blue, red and black lines represent the cell divides in Cases I, II, and III, respectively. t_0 is a unit of simulation time. (For interpretation of the references to color in this figure legend, the reader is referred to the web version of this article.)

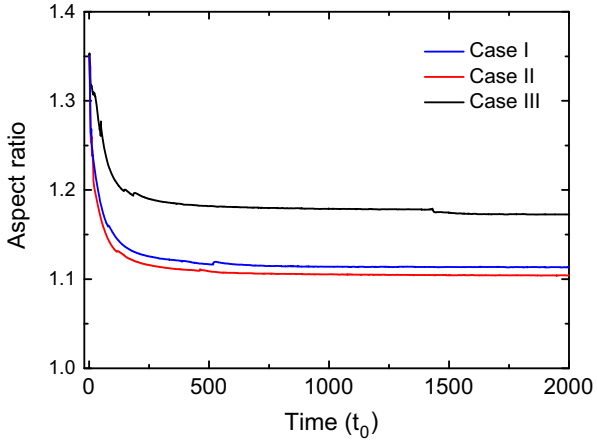

Fig. 8. The average of the aspect ratio of cell shapes as a function of the simulation time t. The blue, red and black lines represent the cell divides in Cases I, II, and III, respectively. t_0 is a unit of simulation time. (For interpretation of the references to color in this figure legend, the reader is referred to the web version of this article.)

indicates that the orientation of cell division depends less sensitively on the cell shape if the molecular contractive strength is weak.

3.2. *Influence of dividing cell on the stress level of its neighboring cells*

The division of cells will lead to a reduction in cell area and in turn, a local topology change. This change in local topology will vary the local stress and gradually affect the global stress of the cell monolayer. To understand the influence of cell division on the monolayer stress, we firstly investigate its effect on the local stress of itself and its neighbors. As an example, we consider the local stress changes in Case II in this subjection.

As illustrated in Fig. 4(a), seven cells form a cluster. The central cell, denoted as a mother (M) cell, will divide into two daughter (D) cells. The division of this mother cell induces a sudden change in geometric shapes, and then, the shape and stress level of

neighboring (N) cells will be affected. We calculate the stresses along the long cell axis of a daughter cell and a neighboring cell, and plot them as a function of time for a short time interval (see Fig. 4(b)). At time $t=0$, the mother cell divides into two daughter cells with the stress σ_{long} decreasing suddenly to a certain value. Then, the daughter cells will grow toward their optimal area, inducing the further decrease in the local stress. Meanwhile, the local stress of the neighboring cell gradually decreases with the time, because the applied extension of the cell 'N' is gradually released by the growth of the cell 'D'.

3.3. Influence of oriented cell division on the global stress of the monolayer

In this subjection, we investigate the global stress of the monolayer after stretch in three cases of cell division. The monolayer stresses σ_{xx} in the tensile direction, calculated by Eq. (8), are plotted with respect to the simulation time (Fig. 5). It can be seen that the stress of the cell monolayer decreases rapidly at tens of simulation time steps. This is because a number of large cells divide after the stretch, and the newly generated cells grow to release the applied extension. The frequent division of cells could release the monolayer stress, as demonstrated in our previous work (Xu et al., 2015). As the time further increases, the monolayer stress decreases slowly and approaches zero at equilibrium in the three cases. Thus, different orientations of cell division does not vary the final stress of the monolayer. However, it should be noticed that the monolayer stress decreases faster in case II than those in other cases. This result means that the orientated cell division along the geometric long axis can effectively dissipate the external stress and lead the monolayer to a homeostatic state quickly.

3.4. Cellular orientation changes responding to the stretch of monolayers

When the monolayer is stretched, some elongated cells divide into daughter cells, and the newly generated cells can grow and resist the extension. During this process, the cell packing geometry within the monolayer will be changed in response to the extension. In the following subsections, we study the changes of the orientation and the aspect ratio of cells responding to the stretch of monolayers.

The packing geometry of cells, dividing along the long axis, is illustrated at different time steps in Fig. 6. The red lines represent the long-axis orientation of the best-fit ellipse of the cell shape. For clarification, the orientations of cells appearing at the box boundaries are not shown. At the onset of stretch, the cell is elongated with an alignment along the tensile direction, as shown in Fig. 6(a). The division of cells will change their alignment orientations, as highlighted in Fig. 6(a) and (b). The cartoon in Fig. 6(a') illustrates that a mother cell with horizontal alignment divides into two daughters with nearly vertical alignment. When more and more cells divide, the orientation of cells within the monolayer seems to be randomly distributed (Fig. 6(c)).

To quantitatively understand the change of cellular orientation during the division in the monolayer, we use an order parameter S to denote the cell alignment (de Gennes and Prost, 1994)

$$S = \langle \cos\ 2\theta \rangle \tag{10}$$

where θ is the cellular orientation and $\langle \cdots \rangle$ denotes the average of all cells within the monolayer. Following this definition, $S=0$ implies that the cells within the monolayer are randomly orientated. $S=1$ and $S=-1$ represent the cells are parallel and perpendicular to the stretching direction, respectively. We plot the order parameter S with respect to the simulation time in three division cases (Fig. 7). It can be seen that S is around 0.9 for all three cases at the beginning, since each cell is elongated along the stretching direction. As the time increases, the value of S gradually decreases because the dividing cells can significantly vary their orientations (see Figs. 6(a) and 6(b)). In Case II, S approaches to zero at equilibrium, meaning that the cells are randomly aligned in the monolayer. In Cases I and III, the values of S are respectively negative and positive, indicating that cells tend to respectively align perpendicularly and parallel to the stretching direction. These results show that the division along the long cell axis is helpful for the formation of random packing geometric shapes of cells in the monolayer.

3.5. Effects of division orientation on the aspect ratio of cells within the monolayer

Wyatt et al. (2015) experimentally showed that the cells within non-stretched and stretched monolayers possessed different aspect ratios when they divided. In this subsection, we study the dependence of the aspect ratio of cells on their division orientation, since the aspect ratio is an important parameter to characterize the cell shape. In this paper, the aspect ratio is defined as the ratio between the long and short axes of cellular ellipses. Fig. 8 shows the average of the aspect ratio of all cells as a function of the time in three division cases. At the beginning, the aspect ratios are the same ($\sim$1.35) in all cases. As the time increases, the aspect ratio decreases toward a constant. It can be seen form Fig. 8 that at equilibrium, the aspect ratio ($\sim$1.17) in case III is larger than those in other two cases ($\sim$1.11). The smaller aspect ratio means a more isotropic geometric shape of cells. If the aspect ratio is 1, the cell is round, and behaves isotropically. Thus, these simulation results demonstrate that the division along long cell axis or the stretch axis can help generate more isotropic cell shapes within a stretched monolayer.

4. Conclusions

In summary, we have studied the effects of the orientation of cell division on the stress and cell packing geometry of a monolayer, when the monolayer is largely stretched. We investigate three cases of orientated cell division: (I) dividing along the stretch axis, (II) dividing along the long cell axis, and (III) dividing at a random orientation. It is found that the division along the long cell axis has a minimal energy difference. The division of the cell induces a sudden decrease in the local stress of itself, and the growth of daughter cells leads their adjacent cells to gradually release the applied stress. After stretch, the global stress of the monolayer decreases more rapidly in Case II that the cell divides along the long axis. Furthermore, the long-axis division results in more random cell orientations and more isotropic cell shapes within the monolayer, comparing with other two cases. This study shows the effects of orientated cell division on the mechanics and configurations of a cell monolayer, and helps understand the role of local cell-level changes in the global properties of epithelial tissues.

Conflict of interest statement

The authors declare that there are no conflicts of interest associated with the present study.

Acknowledgments

Financial supports from the National Natural Science Foundation of China (No. 11402193) and the Fundamental Research Funds for the Central Universities of China are acknowledged.

References

Basan, M., Elgeti, J., Hannezo, E., Rappel, W.-J., Levine, H., 2013. Alignment of cellular motility forces with tissue flow as a mechanism for efficient wound healing. Proc. Natl. Acad. Sci. USA 110, 2452–2459.

Camley, B.A., Zhang, Y., Zhao, Y., Li, B., Ben-Jacob, E., Levine, H., Rappel, W.-J., 2014. Polarity mechanisms such as contact inhibition of locomotion regulate persistent rotational motion of mammalian cells on micropatterns. Proc. Natl. Acad. Sci. USA 111, 14770–14775.

Chen, C.S., Mrksich, M., Huang, S., Whitesides, G.M., Ingber, D.E., 1997. Geometric control of cell life and death. Science 276, 1425–1428.

de Gennes, P.G., Prost, J., 1994. The Physics of Liquid Crystals. Clarendon Press, Oxford.

Farhadifar, R., Röper, J.-C., Aigouy, B., Eaton, S., Jülicher, F., 2007. The influence of cell mechanics, cell-cell interactions, and proliferation on epithelial packing. Curr. Biol. 17, 2095–2104.

Fink, J., Carpi, N., Betz, T., Bétard, A., Chebah, M., Azioune, A., Bornens, M., Sykes, C., Fetler, L., Cuvelier, D., Piel, M., 2011. External forces control mitotic spindle positioning. Nat. Cell Biol. 13, 771–778.

Fletcher, A.G., Osterfield, M., Baker, R.E., Shvartsman, S.Y., 2014. Vertex models of epithelial morphogenesis. Biophys. J. 106, 2291–2304.

Gibson, M.C., Patel, A.B., Nagpal, R., Perrimon, N., 2006. The emergence of geometric order in proliferating metazoan epithelia. Nature 442, 1038–1041.

Gibson, W.T., Veldhuis, J.H., Rubinstein, B., Cartwright, H.N., Perrimon, N., Wayne Brodland, G., Nagpal, R., Gibson, M.C., 2011. Control of the mitotic cleavage plane by local epithelial topology. Cell 144, 427–438.

Graner, F., Glazier, J.A., 1992. Simulation of biological cell sorting using a two-dimensional extended potts model. Phys. Rev. Lett. 69, 2013–2016.

Gray, D., Plusa, B., Piotrowska, K., Na, J., Tom, B., Glover, D.M., Zernicka-Goetz, M., 2004. First cleavage of the mouse embryo responds to change in egg shape at fertilization. Curr. Biol. 14, 397–405.

Guillot, C., Lecuit, T., 2013. Mechanics of epithelial tissue homeostasis and morphogenesis. Science 340, 1185–1189.

Harris, A.R., Peter, L., Bellis, J., Baum, B., Kabla, A.J., Charras, G.T., 2012. Characterizing the mechanics of cultured cell monolayers. Proc. Natl. Acad. Sci. USA 109, 16449–16454.

Harris, A.R., Bellis, J., Khalilgharibi, N., Wyatt, T., Baum, B., Kabla, A.J., Charras, G.T., 2013. Generating suspended cell monolayers for mechanobiological studies. Nat. Protoc. 8, 2516–2530.

Heisenberg, C.-P., Bellaïche, Y., 2013. Force in tissue morphogenesis and patterning. Cell 153, 948–962.

Hofmeister, W., 1863. Zusatze und Berichtigungen zu den 1851 veröffentlichen Untersuchungengen der Entwicklung höherer Kryptogamen. Jahrbucher für Wissenschaft und Botanik. 3, pp. 259–293.

Ishihara, S., Sugimura, K., 2012. Bayesian inference of force dynamics during morphogenesis. J. Theor. Biol. 313, 201–211.

Käfer, J., Hayashi, T., Marée, A.F.M., Carthew, R.W., Graner, F., 2007. Cell adhesion and cortex contractility determine cell patterning in the *Drosophila* retina. Proc. Natl. Acad. Sci. USA 104, 18549–18554.

Kondo, T., Hayashi, S., 2013. Mitotic cell rounding accelerates epithelial invagination. Nature 494, 125–129.

Kuipers, D., Mehonic, A., Kajita, M., Peter, L., Fujita, Y., Duke, T., Charras, G., Gale, J.E., 2014. Epithelial repair is a two-stage process driven first by dying cells and then by their neighbours. J. Cell Sci. 127, 1229–1241.

Lecuit, T., Lenne, P.F., 2007. Cell surface mechanics and the control cell shape, tissue patterns and morphogenesis. Nat. Rev. Mol. Cell Biol. 8, 633–644.

LeGoff, L., Rouault, H., Lecuit, T., 2013. A global pattern of mechanical stress polarizes cell divisions and cell shape in the growing *Drosophila* wing disc. Development 140, 4051–4059.

Li, B., Sun, S.X., 2014. Coherent motions in confluent cell monolayer sheets. Biophys. J. 107, 1532–1541.

Marinari, E., Mehonic, A., Curran, S., Gale, J., Duke, T., Baum, B., 2012. Live-cell delamination counterbalances epithelial growth to limit tissue overcrowding. Nature 484, 542–545.

Minc, N., Burgess, D., Chang, F., 2011. Influence of cell geometry on division-plane positioning. Cell 144, 414–426.

Monier, B., Gettings, M., Gay, G., Mangeat, T., Schott, S., Guarner, A., Suzanne, M., 2015. Apico-basal forces exerted by apoptotic cells drive epithelium folding. Nature 518, 245–248.

Ragkousi, K., Gibson, M.C., 2014. Cell division and the maintenance of epithelial order. J. Cell Biol. 207, 181–188.

Rauzi, M., Verant, P., Lecuit, T., Lenne, P.-F., 2008. Nature and anisotropy of cortical forces orienting *Drosophila* tissue morphogenesis. Nat. Cell Biol. 10, 1401–1410.

Sepúlveda, N., Petitjean, L., Cochet, O., Grasland-Mongrain, E., Silberzan, P., Hakim, V., 2013. Collective cell motion in an epithelial sheet can be quantitatively described by a stochastic interacting particle model. PLoS Comput. Biol. 9, e1002944.

Strauss, B., Adams, R.J., Papalopulu, N., 2006. A default mechanism of spindle orientation based on cell shape is sufficient to generate cell fate diversity in polarised Xenopus blastomeres. Development 133, 3883–3893.

Sugimura, K., Ishihara, S., 2013. The mechanical anisotropy in a tissue promotes ordering in hexagonal cell packing. Development 140, 4091–4101.

Théry, M., Racine, V., Pépin, A., Piel, M., Chen, Y., Sibarita, J.-B., Bornens, M., 2005. The extracellular matrix guides the orientation of the cell division axis. Nat. Cell Biol. 7, 947–953.

Tzur, A., Kafri, R., LeBlue, V.S., Lahav, G., Kirschner, M.W., 2009. Cell growth and size homeostasis in proliferating animal cells. Science 325, 167–171.

Wilk, G., Iwasa, M., Fuller, P.E., Kandere-Grzybowska, K., Grzybowski, B.A., 2014. Universal area distributions in the monolayers of confluent mammalian cells. Phys. Rev. Lett. 112, 138104.

Wyatt, T.P.J., Harris, A.R., Lam, M., Cheng, Q., Bellis, J., Dimitracopoulos, A., Kabla, A. J., Charras, G.T., Baum, B., 2015. Emergence of homeostatic epithelial packing and stress dissipation through divisions oriented along the long cell axis. Proc. Natl. Acad. Sci. USA 112, 5726–5731.

Xu, G.K., Liu, Y., Li, B., 2015. How do changes at the cell level affect the mechanical properties of epithelial monolayers? Soft Matter 11, 8782–8788.